analytical chemistry

Article

Cite This: Anal. Chem. 2019, 91, 6200−6205

pubs.acs.org/ac

Nanoparticle Analysis in Biomaterials Using Laser Ablation−Single Particle−Inductively Coupled Plasma Mass Spectrometry

Dino Metarapi,[†,‡] Martin Šala,[†] Katarina Vogel-Mikuš,[§,∥] Vid S. Šelih,[†] and Johannes T. van Elteren*[,†]

[†]Department of Analytical Chemistry, National Institute of Chemistry, Hajdrihova 19, SI-1000 Ljubljana, Slovenia
[‡]Faculty of Chemistry and Chemical Technology, University of Ljubljana, Večna pot 113, SI-1001 Ljubljana, Slovenia
[§]Department of Biology, Biotechnical Faculty, University of Ljubljana, Jamnikarjeva 101, SI-1000 Ljubljana, Slovenia
[∥]Jožef Stefan Institute, Jamova 39, SI-1000 Ljubljana, Slovenia

Supporting Information

ABSTRACT: In the past decade, the development of single particle−inductively coupled plasma mass spectrometry (SP-ICPMS) has revolutionized the field of nanometallomics. Besides differentiation between dissolved and particulate metal signals, SP-ICPMS can quantify the nanoparticle (NP) number concentration and size. Because SP-ICPMS is limited to characterization of NPs in solution, we show how solid sampling by laser ablation (LA) adds spatial-resolution characteristics for localized NP analysis in biomaterials. Using custom-made gelatin standards doped with dissolved gold and commercial or synthesized gold nanoparticles, LA-SP-ICPMS conditions such as laser fluence, beam size, and dwell time were optimized for NP analysis to minimize NP degradation, peak overlap, and interferences from dissolved gold. A data-processing algorithm to retrieve the NP number concentration and size was developed for this purpose. As a proof-of-concept, a sunflower-root-sample cross-section, originating from a sunflower plant exposed to gold NPs, was successfully imaged using the optimized LA-SP-ICPMS conditions for localized NP characterization.

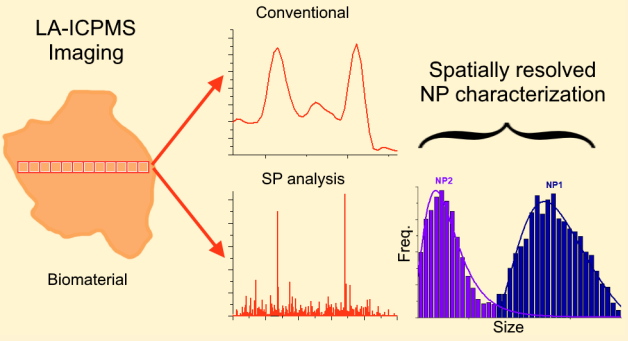

With the growing use of nanoparticles (NPs) in different fields such as energy production,[1] biology, medicine,[2,3] and consumer goods,[4] more and more concerns have been raised about their safety.[5] Because living systems have different uptake mechanisms for NPs compared to dissolved species,[6,7] potential risks exist for human health through inhalation exposure and dermal exposure.[8] Growing awareness has led to a sharp increase in NP studies and development of methods for the measurement of NPs.[9] Methods such as atomic-force microscopy (AFM),[10] scanning electron microscopy (SEM),[11] secondary-ion mass spectrometry (SIMS),[12] transmission electron microscopy (TEM), dynamic light scattering (DLS),[13,14] and single particle−inductively coupled plasma mass spectrometry (SP-ICPMS) are frequently used to characterize NPs.

The last method has become a well-established method for simultaneous determination of particle size and number concentration.[15,16] However, a limitation of this technique is that solid samples that contain NPs have to be dissolved and subsequently suspended for analysis. Thus, the spatial-distribution information on particles in solid samples is lost, and the experimenter runs the risk of affecting the integrity of the particles during sample preparation. LA-ICPMS can be used to measure the spatial distribution of nanoparticles in biological tissues[17−19] or serve as a technique to monitor NP-tagged antibodies.[20] NPs have even been sized by thin-layer chromatography (TLC) and measured by LA-ICPMS.[21] However, individual NPs were identified in none of these papers; to our knowledge, only Donard et al.[22] have shown the detection of discrete, single NP events upon ablation of a solid material.

This work focuses on the development of an LA-SP-ICPMS method for nanoparticle analysis in biomaterials and on defining the limitations of the method for the measurement of NPs. Custom-made gelatin standards containing commercial or synthesized gold NPs of various sizes and with different number concentrations were used to optimize the conditions for measurement of gold NPs. By increasing the dissolved-gold concentration, we established the method's sizing threshold because nanoparticles are always generated upon ablation of dissolved species. LA-SP-ICPMS conditions such as laser-beam size, laser fluence, and dwell time were varied to optimize the method.

Received: February 15, 2019
Accepted: March 30, 2019
Published: March 31, 2019

The optimized method was used to measure gold-NP size, number concentration, and localization in roots of sunflower plants grown hydroponically with gold NPs added.

EXPERIMENTAL SECTION

Gold-Nanoparticle Synthesis and Characterization. Gold NPs of progressively increasing diameter were synthesized using a modified Turkevich method[23,24] by reduction of Au^{3+} in an aqueous solution of $HAuCl_4$ with trisodium citrate. By consecutively growing the particles and controlling the reaction conditions, nine particle sizes with diameters from ~20 to ~100 nm were synthesized. Mean diameters of the synthesized particles were determined by routine methods using dynamic light scattering (DLS, Zetasizer Nano ZS, Malvern, Almelo, Netherlands) and SP-ICPMS (Single Nanoparticle Analysis Module, Agilent 7900, Agilent Technologies, Santa Clara, CA) yielding the following nine sizes (mean ± SD): 26 ± 5, 33 ± 5, 37 ± 6, 40 ± 5, 47 ± 6, 54 ± 6, 65 ± 8, 80 ± 9, and 86 ± 9 nm. Gold-NP standards with mean sizes of 20 nm (7.00×10^{11} particles mL^{-1}), 40 nm (9.00×10^{10} particles mL^{-1}), 60 nm (2.60×10^{10} particles mL^{-1}), and 100 nm (5.60×10^{9} particles mL^{-1}), all with less than 8% variability, from BBI Solutions (Cardiff, U.K.) were used in the characterization of the synthesized gold NPs. NPs were diluted in ultrapure deionized water prior to measurement. Transmission electron microscopy (TEM, ARM 200 CF, Jeol, Akishima, Japan) was used to investigate the morphology of the NPs synthesized.

Preparation of Gelatin Standards for NP Analysis. Preparation of homogeneous NP standards for LA-SP-ICPMS analysis was carried out by suspending gold NPs, commercially obtained or custom-synthesized, in 10% (m/v) gelatin (porcine-skin gelatin, type A, bloom strength 300, Sigma-Aldrich, St. Louis, MO) by ultrasonication for 1 min. The gelatin was heated to 55 °C prior to the addition of the gold NPs and then drop-casted on a glass microscope slide, after which the gelatin droplets were dried in a convection oven at 100 °C for 1 h, similar to an earlier reported method for preparation of dissolved (elemental) standards.[25] Supporting Information Section 1 (SI-1) demonstrates the homogeneous distribution of NPs in the gelatin standards.

Cultivation of Plants in NP-Spiked Hydroponics and Root-Sample Preparation. Sunflower seeds were sterilized in 10% H_2O_2 and planted in vermiculite. After 10 days, 5 cm seedlings were transferred to tubes containing 100 mL of Hoagland solution. After 1 week of adjustment in hydroponics, 10 plants were exposed for 8 days to gold NPs (60 nm gold NPs, 1.83×10^{9} NP mL^{-1}, citrate stabilized, <12% variability, Sigma-Aldrich, St. Louis, MO) in 100 mL of Hoagland solution. As controls, 10 plants were grown in Hoagland solution without NPs. Sunflowers were kept in a growing chamber at 22 °C with a 16/8 day−night photoperiod and 60% humidity. SI-2 gives the anatomical cross-sectional structure of a sunflower root. At the end of the experiment, the plants were taken from the tubes, and the roots were rinsed with distilled water. The rootlets were detached from the plant, inserted in a stainless-steel needle, and flash-frozen in propane cooled with liquid nitrogen.[26] Subsequently, the roots were cryotomed (cryostat Leica CM5030S, Wetzlar, Germany) to 20 μm thick slices, deposited on parafilm, and freeze-dried (Alpha 2-4, Martin Christ Gefriertrocknungsanlagen, Osterode am Harz, Germany).

LA-SP-ICPMS Instrument and Operating Conditions for NP Analysis. All NP-analysis measurements were conducted with an Analyte G2, 193 nm ArF* LA instrument (Teledyne Photon Machines Inc., Bozeman, MT) with a two-volume ablation cell (HelEx II; He carrier gas flow rate, cup = 0.5 l min^{-1}, cell = 0.3 l min^{-1}). The LA unit was interfaced with an ICPMS instrument (Agilent 7900, Agilent Technologies, Santa Clara, CA). The ICPMS was operated in time-resolved analysis mode with a dwell time of 100 μs, acquiring the mass of ^{197}Au. A typical gold-nanoparticle event in the ICPMS lasts ca. 500 μs;[27] the minimum selectable dwell time of 100 μs was chosen to record this transient signal. When the sensitivity of the ICPMS is adequate, this gives us sufficient resolution to distinguish a double event, in which two particles are recorded, from a single event. Furthermore, it allows measurement of single NPs in an LA-packet densely packed with NPs originating from a HelEx II laser-ablation cell. Gelatin NP standards and sunflower-root-sample cross-sections were subjected to laser ablation via a line-scan routine.

An NP-analysis protocol was developed for retrieval of the NP number concentration and size by optimizing the laser-ablation conditions using the NP standards. To this end, LA-SP-ICPMS conditions were varied as follows: fluence, 0.5−4 J cm^{-2}; laser-beam size, 10−85 μm (round or square mask); and dwell time, 100−1000 μs. Because NPs are also generated upon ablation of dissolved species in the matrix, we studied the influence of the dissolved-gold concentration on the detection of gold NPs to establish a sizing threshold. Additionally, mixed NP standards with three NP sizes were used to prove the performance of the NP-analysis protocol for accurate NP sizing.

The optimized laser-ablation conditions for the sunflower-root cross-sections were as follows (for ablation of the complete thickness): beam diameter, 5 μm (square mask); scanning speed, 25 μm s^{-1}; fluence, 0.4 J cm^{-2}; repetition rate, 50 Hz; and dwell time, 100 μs. These conditions imply that laser ablation took place every 0.5 μm along the line during line scanning; by gathering the total counts in every subsequent 10 shots (i.e., the total counts in 2000 data points), a conventional gold map resulted with a pixel size of 5 × 5 μm^2. By more detailed processing of the data, each time-resolved peak in the line scan can be associated with a single nanoparticle, with the height of the peak corresponding to the particle mass or particle size. Thus, not only the distribution of gold in the tissue can be derived but also the particle number concentration and size at a particular location.

Data Processing. The raw time-resolved-analysis data from ablation of the gelatin NP standards and sunflower-root-sample cross-sections were processed with Origin software (Origin 2018, OriginLab Corporation, Northampton, MA). Line-scan data were subjected to peak analysis by integration of individual peaks, followed by creation of a histogram using the peak areas. The histogram shows us the presence of dissolved species and how many different NP sizes are present; the number of peaks for a certain NP size is indicative of the particle number concentration. When the dissolved-gold concentration increases, NP analysis of small NPs becomes a problem (see the Results and Discussion section). Histograms can be created from a complete line scan, a fraction of a line scan, or even a single laser-ablation shot when enough NP peaks are generated per shot. Thus, the NP number concentration in the standards or root sample determines what kind of spatial resolution is possible in element maps with

DOI: 10.1021/acs.analchem.9b00853
Anal. Chem. 2019, 91, 6200−6205

regard to NP sizing, as enough NP-detection events (>200) are essential to produce a suitable histogram for retrieval of the NP size. Selection of the proper bin size in the histograms is critical for proper fitting of the data with a log-normal distribution curve; we used the Shimazaki and Shinomoto method for bin-size optimization, as this method does not require assumptions about the distribution function.[28] The centers of the fitted log-normal distribution curves correspond to the mean sizes of the gold NPs. SI-3 gives a schematic overview of the data-processing workflow.

RESULTS AND DISCUSSION

Concept of NP Analysis by LA-SP-ICPMS. The raw data collected by LA-SP-ICPMS requires substantial processing and an in-depth understanding of the events occurring both during the laser-ablation process and in the ICPMS detection step. Figure 1 illustrates the concept of NP analysis in biomaterials,

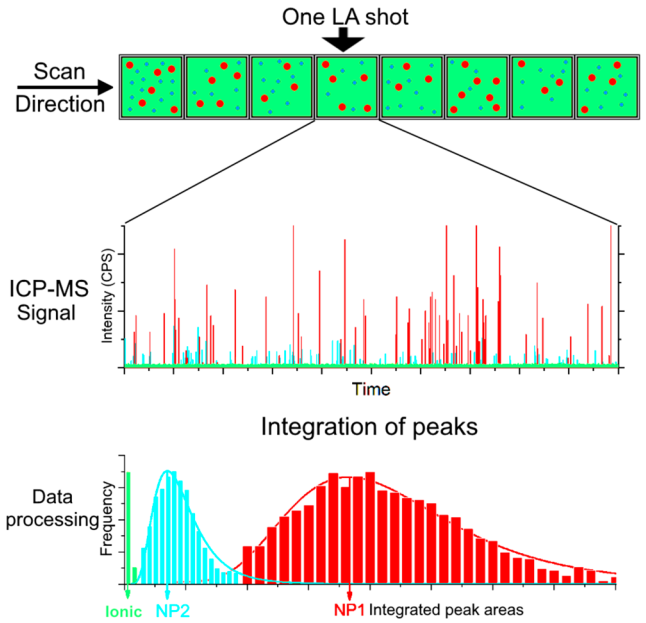

Figure 1. Concept of NP analysis in biomaterials using LA-SP-ICPMS. Homogeneously distributed dissolved species are represented by a green background, whereas the two different NP sizes are shown as red (diameter of d) and blue (diameter of $d/2$) dots.

from ablation to detection to processing. A single line scan is shown along which single "squares", associated with pulses from a laser beam with a square mask, are subjected to NP analysis. The highlighted square contains dissolved species and NPs of two sizes, all correlated with the same element. The diameter of NP1 is twice the diameter of NP2, but their particle number concentration is the same. The ICPMS trace, recorded with a dwell time of 100 μs, shows the background generated by the dissolved species and the two different particle sizes, as evidenced from the peaks with roughly two different heights (the average height ratio is 8 as a result of cubic conversion of NP size to mass). The numbers of peaks for the different sizes are similar because of their equal number concentrations. After subtraction of the dissolved-species background from the raw signal, integration of all peaks, counting of peaks, and sorting of peaks by incidence, a histogram is created showing the three possible particle sizes: (from left to right) dissolved species, NP2, and NP1.

The individual histograms are fitted with log-normal distributions, as modeling has shown that particles are not monodisperse but follow a log-normal distribution based on a kinetic approach, assuming normally distributed times for growth and destruction of particles.[29] The positions of the individual peaks (μ) correspond to the mean particle sizes (given in peak-area units, i.e., counts). The particle number concentration can be retrieved from the cumulated incidences for each NP size divided by the detection-efficiency factor (DEF), which takes into account the losses induced by ablation, transport, atomization ionization, and counting. This detection-efficiency factor can be defined as DEF = (mean number of particles per shot detected by SP-ICPMS)/(mean number of particles per shot in the mass ablated). The number of particles per shot in the mass ablated is calculated from the area ablated × depth × matrix density × particle number concentration. The area ablated is associated with the beam size, and the average depth per pulse on gelatin is 156 ± 7 nm, as measured by confocal microscopy. Using Figure 1 as a guideline, a number of parameters (laser fluence, laser-beam size, dissolved-species concentration, and dwell time) were varied for optimization of the NP-analysis protocol using NP standards.

Influence of Various LA-SP-ICPMS Parameters on NP Analysis. To find the optimal laser fluence for analysis of NPs (i.e., with minimal degradation of the particles and thus negligible effect on the mean particle size), NP standards containing 40 nm gold particles in gelatin were subjected to line scanning with various fluences. From the histograms in SI-4, it can be seen how a higher fluence not only leads to an increase of the total number of NPs detected but also to a shift to smaller, degraded NPs. The mean size of the original NPs does not seem to change much with increasing fluence. However, with increasing fluence, the dip between the smaller, degraded particles and the original NPs becomes less and less pronounced, indicating the formation of a range of NP sizes. This is further illustrated in Figure 2 where the ratio between smaller, degraded NPs and original NPs is plotted against the fluence. It is clear that a low fluence ($\leqslant$ 1 J cm^{-2}) needs to be used for NP analysis to minimize degradation of NPs and to retrieve the correct mean particle size.

Using an adequate laser fluence, ablation of NPs initially present in biomaterials leads to the release of intact NPs (i.e.,

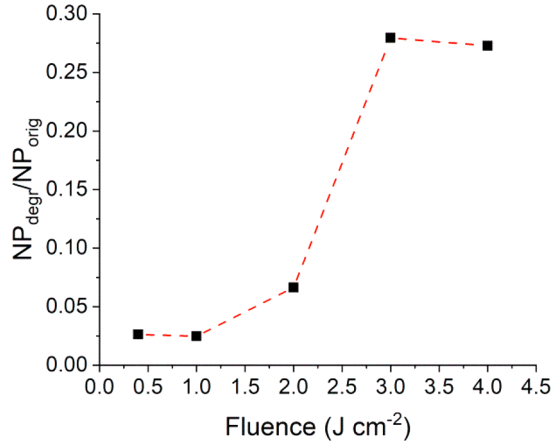

Figure 2. Partial conversion of 40 nm gold nanoparticles in gelatin (NP_{orig}) to smaller, degraded nanoparticles (NP_{degr}) as a function of the laser fluence.

DOI: 10.1021/acs.analchem.9b00853
Anal. Chem. 2019, 91, 6200−6205

NPs that are incorporated in the broad range of nano- to microparticles[30] generated upon ablation of the matrix). This implies that upon increasing the laser-beam size, more similarly sized intact NPs are released from the matrix. This is illustrated in Figure 3, showing how the laser-beam size (10, 20, 35, 50,

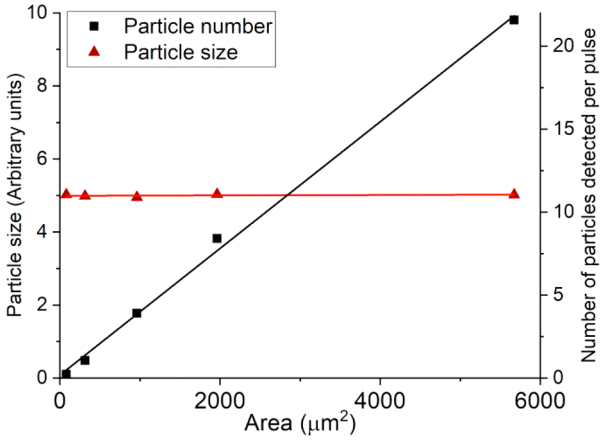

Figure 3. Numbers of NPs and their mean sizes per laser-ablation pulse as detected by ICPMS upon ablation of a gelatin standard containing 40 nm gold NPs with a number concentration of 9.0×10^{10} g^{-1} as a function of the area ablated per pulse. Areas are associated with beam sizes of 10, 20, 35, 50, and 85 μm (round mask).

and 85 μm, round mask) influences the number of NPs detected by the ICPMS and their mean size upon ablation of a gelatin standard with 40 nm gold NPs and a NP number concentration of 9.0×10^{10} g^{-1}. As expected, the number of particles detected is linearly proportional to the area ablated per laser pulse, whereas the mean particle size stays roughly the same. The detection-efficiency factor, DEF, calculated from the ratio of the number of NPs detected by the ICPMS and the number of NPs contained in the volume ablated, is 0.19 ± 0.07. In principle, a reduction of the beam size can serve as a "dilution" and thus a straightforward way to avoid detection of double peaks. The same effect may be obtained by reducing the repetition rate (data not shown).

Laser ablation of dissolved species involves the creation of many small NPs, in contrast to laser ablation of NPs, in which the NPs are merely released from the biomaterial. When the number concentration of NPs initially present in the biomatrix increases, the peak density detected by ICPMS increases, whereas the peak height and area stay the same. When the dissolved-species concentration in the biomatrix increases, the mean NP size of the particles generated is affected negligibly. However, the mean dissolved-species concentration increases proportionally with the dissolved-species concentration, leading to a higher background. Thus, at higher dissolved-species concentrations in biomatrices, the detection of NPs may be negatively affected when the "background noise" caused by the dissolved species cannot be differentiated from the NP signals, leading to inaccurate NP analysis. Figure 4 shows (zoomed-in) raw line-scan data for gelatin standards containing 10, 20, and 50 μg g^{-1} dissolved gold and for gelatin standards containing 26 and 37 nm gold nanoparticles. It is evident that the presence of 50 μg g^{-1} dissolved gold may already start influencing the measurement of the smaller NPs of 26 nm. However, because the results in Figure 4 are based on laser ablation with a 35 μm beam size (square mask),

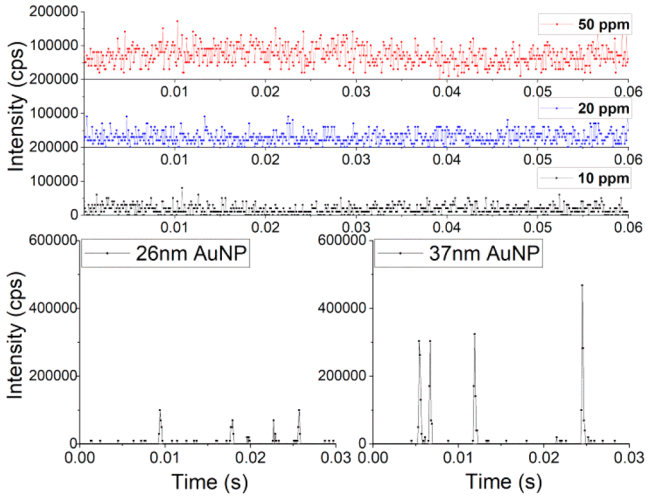

Figure 4. Raw (zoomed-in) line-scan data for gelatin standards containing 10, 20, and 50 μg g^{-1} dissolved gold (A) and gelatin standards containing 26 and 37 nm gold nanoparticles (B).

dilution by reducing the beam size will not affect the heights or areas of the NP peaks, but the dissolved-species signal will decrease in a squared fashion associated with the area ablated. However, this dilution step will affect the peak density, so the particle number concentration in the gelatin needs to be sufficiently high to perform this step. If for this reason dilution is not possible, a threshold needs to be established on the basis of 5 standard deviations of the dissolved-species signal.[31] In Figure 4, this would mean thresholds of 71 000, 105 000, and 202 000 cps for the respective dissolved-species concentrations of 10, 20, and 50 μg g^{-1}. These thresholds would then serve as baseline signals to be extracted from the NP peak signals prior to integration. For real-world applications where materials with inhomogeneously distributed dissolved species are ablated, we determined the threshold by applying a median filter across the entire line scan; this was followed by calculating the threshold on the basis of counting statistics in each median data point, P, associated with the counts in the integration window: $P + 5\sqrt{P}$.

One of the critical LA-SP-ICPMS parameters for NP analysis is the dwell time[22,32] (i.e., the integration window the ICPMS uses to accumulate counts). Especially when the NP number concentration is high, and no further instrumental dilution is possible, the probability to encounter more than one peak in the integration window increases, and inaccurate NP analysis ensues.[33] To show this effect, a gelatin standard with 40 nm gold NPs and a NP number concentration of 9.0×10^{10} g^{-1} was ablated (beam size, 85 μm (round mask); repetition rate, 20 Hz; scanning speed, 40 μm s^{-1}), and the counts associated with ^{197}Au were accumulated with integration windows of 100, 500, and 1000 μs. In Figure 5, the histograms obtained after extraction of the NP-sizing data associated with the line scans on the gelatin are shown for the different integration windows. It is evident from the histograms that at least two NP sizes are recorded for dwell times of 500 and 1000 μs, the second peak as a result of false-positive detection of two NP events that cannot be distinguished in postprocessing. From fitting, it follows that the areas associated with these two sizes are 87 and 13% (for a dwell time of 500 μs) and 72 and 28% (for a dwell time of 1000 μs); that is, the probabilities of recording a double NP event are 13% (500 μs)

DOI: 10.1021/acs.analchem.9b00853
Anal. Chem. 2019, 91, 6200−6205

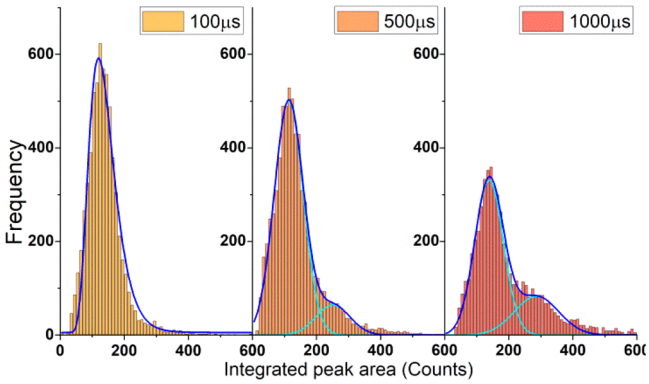

Figure 5. NP sizing for different dwell times upon ablation of a gelatin standard containing NPs with a mean size of 40 nm and a particle number concentration of 9.0×10^{10} g^{-1}. The histogram for 100 μs was fitted with a log-normal distribution. For dwell times of 500 and 1000 μs, we performed peak deconvolution to show the increased likelihood of false-positive detection events (double peaks) with increasing dwell time.

and 28% (1000 μs). The mean of the fitted double peaks occurs at ca. twice the integrated peak area for dwell times of 500 and 1000 μs.

SI-5 shows how sizing of the nine synthesized NP gelatin standards by LA-SP-ICPMS compares with sizing of the nine synthesized NP aqueous standards by routine solution SP-ICPMS. A linear relationship is observed, implying that the developed LA-SP-ICPMS NP-sizing method is able to produce accurate results. TEM analysis of one of the synthesized NPs (26 μm) shows the morphology of these particles. To verify whether or not mixed NP sizes can be distinguished, a gelatin standard containing synthesized gold NPs with mean sizes of 86, 47, and 26 nm and respective particle number concentrations of 3.2×10^5, 4.2×10^5, and 3.1×10^6 g^{-1} was subjected to NP sizing using the optimized LA-SP-ICPMS parameters. From Figure 6, it can be seen that these NPs can indeed be separated in a mixed standard, with mean particle sizes matching those of the individual NP standards, enhancing the applicability of this NP-analysis method for real samples. In SI-6, we calculated that under these conditions of virtually no dissolved gold, the minimum NP size measurable was ca. 15 nm.

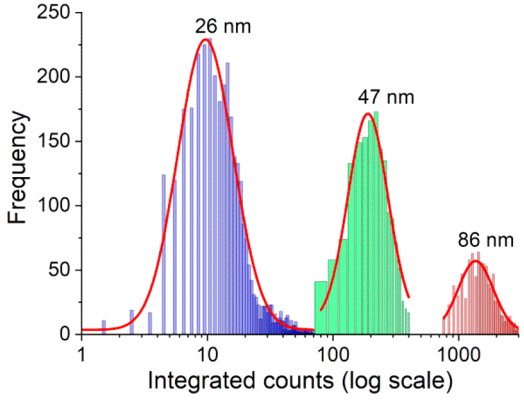

Figure 6. NP sizing of a mixture of synthesized gold NPs in gelatin with mean sizes of 86, 47, and 26 nm and respective particle number concentrations of 3.2×10^5, 4.2×10^5, and 3.1×10^6 NP g^{-1}. Different optimized bin sizes were used in the three histograms.

Demonstration of LA-SP-ICPMS NP Analysis in Real Samples. Root cross-sections originating from sunflower plants exposed to gold NPs with a mean size of 60 nm were subjected to LA-SP-ICPMS NP analysis. The whole root cross-section was analyzed via the method optimized above with the conditions given in the Experimental Section. Parallel, adjoining line scans (100 in total) with 307 000 data points per line scan where manipulated in ImageJ 1.52h[34] to yield a conventional gold map with a pixel size of 5×5 μm^2. Figure 7

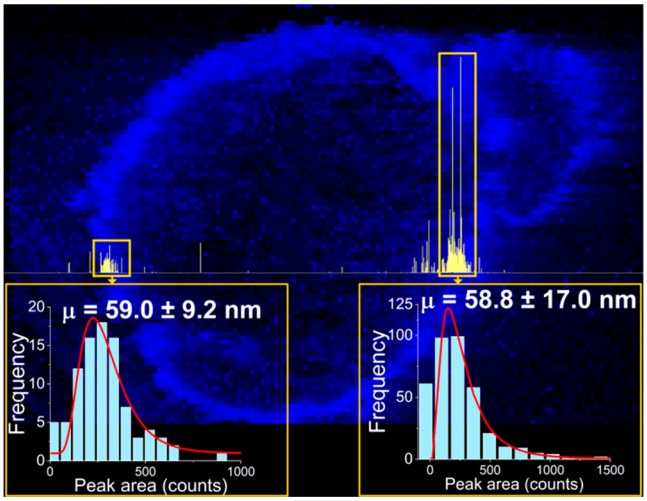

Figure 7. Image (in blue) showing the distribution of gold in a root cross-section from a sunflower plant exposed to gold NPs with a mean size of 60 nm, overlaid with a high-resolution time-resolved signal of a single LA-SP-ICPMS line scan (in yellow). The high gold signals corresponding to the rhizodermis of the root were subjected to NP analysis according to the data-processing procedure in the Data Processing section. The pixel size in the image is 5×5 μm^2, and the line-scan signal was recorded every 100 μs.

shows that gold is mainly distributed on the root surface (plaque) and rhizodermis, and after applying NP sizing on the root-surface and rhizodermis sections indicated, a mean NP size is found that resembles the initial NP size closely. This suggests that gold NPs are likely adsorbed to cell-wall fibrils, thereby decreasing their mobility from the rhizodermis to the cortex and central cylinder. In addition, the results show that NPs are not degraded by plant exudates but retain their original size. By converting the number of shots on the respective rhizodermis sections to mass of matrix ablated, taking into account a detection-efficiency factor (DEF) of 0.19, the NP number concentrations were found to be 6.0×10^{11} and 1.5×10^{11} g^{-1}. In summary, the developed LA-SP-ICPMS method may initiate new research related to nanoparticle interactions in biological systems and nanotoxicology by providing spatially resolved in situ information on NPs.

CONCLUSIONS

We demonstrated how LA-SP-ICPMS can be used as a method for in situ characterization of NPs in biomaterials. Optimization experiments with gold nanoparticles in gelatin showed that a conventional two-volume ablation cell suffices to distinguish individual nanoparticle events upon measurement with a detector capable of dwell times as low as 100 μs. However, it is critical that the laser fluence is kept below 1 J cm^{-2} to avoid NP degradation and that the NPs arriving at the ICPMS are constrained so as to prevent detection of double

DOI: 10.1021/acs.analchem.9b00853
Anal. Chem. 2019, 91, 6200−6205

NP events. Constrainment can be achieved by instrumental dilution via decreasing the beam size or repetition rate. Nevertheless, dissolved-gold species may interfere in the detection of NPs when the noise in this background starts to compete with the NP signals. Provided these LA-SP-ICPMS NP-sizing conditions are met, even NPs of mixed size can be distinguished below 100 nm, the maximum size for particles to be called NPs. The minimum detectable gold-NP size is ca. 15 nm in the presence of negligible amounts of dissolved gold species. LA-SP-ICPMS NP analysis of gold NPs in root cross-sections of sunflower plants that were exposed to 60 nm gold NPs in hydroponics showed the real-world applicability of the technique.

■ ASSOCIATED CONTENT

Supporting Information

The Supporting Information is available free of charge on the ACS Publications website at DOI: 10.1021/acs.analchem.9b00853.

Homogeneity of the gelatin standards, information on root morphology, data processing, NP degradation as a function of laser fluence, validation of NP sizing by LA-SP-ICPMS, determination of measurement yield, and estimation of minimum detectable nanoparticle size (PDF)

■ AUTHOR INFORMATION

Corresponding Author

*E-mail: elteren@ki.si.

ORCID

Dino Metarapi: 0000-0003-0524-0487
Martin Šala: 0000-0001-7845-860X
Vid S. Šelih: 0000-0002-2433-5249
Johannes T. van Elteren: 0000-0003-2237-7821

Notes

The authors declare no competing financial interest.

■ ACKNOWLEDGMENTS

The authors acknowledge financial support from the Slovenian Research Agency (ARRS), contract numbers P1-0034 and N1-0060(C). The first author is a Ph.D. fellow of the ARRS. The authors would like to thank Dr. Samo B. Hocevar for constructive discussions and Dr. Goran Dražić for TEM measurements.

■ REFERENCES

(1) Gowda, S. R.; Leela Mohana Reddy, A.; Zhan, X.; Ajayan, P. M. *Nano Lett.* **2011**, *11* (8), 3329−3333.
(2) Jain, P. K.; Huang, X.; El-sayed, I. H.; El-Sayed, M. A. *Acc. Chem. Res.* **2008**, *41* (12), 1578−1586.
(3) Giljohann, D. A.; Seferos, D. S.; Daniel, W. L.; Massich, M. D.; Patel, P. C.; Mirkin, C. A. *Angew. Chem., Int. Ed.* **2010**, *49* (19), 3280−3294.
(4) Luechinger, N. A.; Athanassiou, E. K.; Stark, W. *Nanotechnology* **2008**, *19* (44), 445201.
(5) Srivastava, V.; Gusain, D.; Sharma, Y. C. *Ind. Eng. Chem. Res.* **2015**, *54* (24), 6209−6233.
(6) Liu, X. Q.; Tang, R. Z. *Drug Delivery* **2017**, *24* (0), 1−15.
(7) Farkas, J.; Christian, P.; Gallego-Urrea, J. A.; Roos, N.; Hassellöv, M.; Tollefsen, K. E.; Thomas, K. V. *Aquat. Toxicol.* **2011**, *101* (1), 117−125.
(8) Gwinn, M. R.; Vallyathan, V. *Environ. Health Perspect.* **2006**, *114*, 1818−1825.
(9) Stephan, C.; Thomas, R. *Spectroscopy* **2017**, *32* (3), 12−25.
(10) Klapetek, P.; Valtr, M.; Nečas, D.; Salyk, O.; Dzik, P. *Nanoscale Res. Lett.* **2011**, *6*, 1−9.
(11) Beveridge, J. S.; Stephens, J. R.; Williams, M. E. *Analyst* **2011**, *136* (12), 2564−2571.
(12) Liang, C.-K.; Eller, M. J.; Verkhoturov, S. V.; Schweikert, E. A. *J. Am. Soc. Mass Spectrom.* **2015**, *26* (8), 1259−1265.
(13) Hagendorfer, H.; Kaegi, R.; Parlinska, M.; Sinnet, B.; Ludwig, C.; Ulrich, A. *Anal. Chem.* **2012**, *84* (6), 2678−2685.
(14) Souza, T. G. F.; Ciminelli, V. S. T.; Mohallem, N. D. S. *J. Phys.: Conf. Ser.* **2016**, *733* (1), 012039.
(15) Degueldre, C.; Favarger, P. Y.; Wold, S. *Anal. Chim. Acta* **2006**, *555* (2), 263−268.
(16) Laborda, F.; Bolea, E.; Jiménez-Lamana, J. *Anal. Chem.* **2014**, *86* (5), 2270−2278.
(17) Cruz-Alonso, M.; Fernandez, B.; Álvarez, L.; González-Iglesias, H.; Traub, H.; Jakubowski, N.; Pereiro, R. *Microchim. Acta* **2018**, *185* (1), 64.
(18) Pisonero, J.; Bouzas-Ramos, D.; Traub, H.; Cappella, B.; Álvarez-Llamas, C.; Richter, S.; Mayo, J. C.; Costa-Fernandez, J. M.; Bordel, N.; Jakubowski, N. *J. Anal. At. Spectrom.* **2019**, *34*, 655−663.
(19) Li, Q.; Wang, Z.; Mo, J.; Zhang, G.; Chen, Y.; Huang, C. *Sci. Rep.* **2017**, *7* (1), 2965.
(20) Tvrdonova, M.; Vlcnovska, M.; Vanickova, L. P.; Kanicky, V.; Adam, V.; Ascher, L.; Jakubowski, N.; Vaculovicova, M.; Vaculovic, T. *Anal. Bioanal. Chem.* **2019**, *411* (3), 559−564.
(21) Yan, N.; Zhu, Z.; Jin, L.; Guo, W.; Gan, Y.; Hu, S. *Anal. Chem.* **2015**, *87* (12), 6079−6087.
(22) Donard, A.; Claverie, F.; Pointurier, F.; Blitz Frayret, C.; Svatosova, B.; Pécheyran, C. *Anal. Chem.* **2017**, *89* (17), 8791−8799.
(23) Turkevich, J.; Stevenson, P. C.; Hillier, J. *Discuss. Faraday Soc.* **1951**, *11*, 55−75.
(24) Bastús, N. G.; Comenge, J.; Puntes, V. *Langmuir* **2011**, *27*, 11098.
(25) Šala, M.; Šelih, V. S.; Van Elteren, J. T. *Analyst* **2017**, *142* (18), 3356−3359.
(26) Vogel-Mikuš, K.; Pongrac, P.; Pelicon, P. *Int. J. PIXE* **2014**, *24* (03n04), 217−233.
(27) Montaño, M. D.; Olesik, J. W.; Barber, A. G.; Challis, K.; Ranville, J. F. *Anal. Bioanal. Chem.* **2016**, *408* (19), 5053−5074.
(28) Shimazaki, H.; Shinomoto, S. *Neural Comput.* **2007**, *19* (6), 1503−1527.
(29) Kiss, L. B.; Söderlund, J.; Niklasson, G. A.; Granqvist, C. G. *Nanotechnology* **1999**, *10* (1), 25−28.
(30) Kuhn, H.-R.; Koch, J.; Hergenröder, R.; Niemax, K.; Kalberer, M.; Günther, D. *J. Anal. At. Spectrom.* **2005**, *20* (9), 894−900.
(31) Tuoriniemi, J.; Cornelis, G.; Hassellöv, M. *Anal. Chem.* **2012**, *84* (9), 3965−3972.
(32) Hineman, A.; Stephan, C. *J. Anal. At. Spectrom.* **2014**, *29* (7), 1252−1257.
(33) Laborda, F.; Jiménez-Lamana, J.; Bolea, E.; Castillo, J. R. *J. Anal. At. Spectrom.* **2013**, *28* (8), 1220−1232.
(34) Schneider, C. A.; Rasband, W. S.; Eliceiri, K. W. *Nat. Methods* **2012**, *9*, 671.

DOI: 10.1021/acs.analchem.9b00853
Anal. Chem. 2019, 91, 6200−6205